Impact of particle size of lithium manganese oxide on charge transfer resistance and contact resistance evaluated by electrochemical impedance analysis

Kingo Ariyoshi, Masumi Tanimoto, Yusuke Yamada

Impact of Particle Size of Lithium Manganese Oxide on Charge Transfer Resistance and Contact Resistance Evaluated by Electrochemical Impedance Analysis

Kingo Ariyoshi*, Masumi Tanimoto, Yusuke Yamada

Department of Applied Chemistry and Bioengineering, Graduate School of Engineering, Osaka City University, 3-3-138 Sugimoto, Sumiyoshi-ku, Osaka, 558-8585, Japan

*Corresponding author.

Email: ariyoshi@osaka-cu.ac.jp (K.A.).

Abstract

To achieve high-power lithium-ion batteries, resistances of both positive and negative electrodes must be reduced, because these are the main sources of internal resistance of the batteries. It is necessary to elucidate the impact of physicochemical properties of lithium insertion materials on the resistance of electrodes, to reduce the internal resistance of the batteries. The resistance of electrodes consists of charge transfer resistance, R_{ct}, and contact resistance, R_{cont}. The diluted electrode method, in which the amount of active material in an electrode varies but retains the factors related to electrode structure, can distinguish the two resistances, R_{ct} and R_{cont}. As this method does not alter the electrode structure, it is possible to elucidate the relationship between the two resistances and the physicochemical properties of lithium insertion materials. In this study, the impact of the particle size of $Li[Li_{0.1}Mn_{1.9}]O_4$ (LMO) on the R_{ct} and R_{cont} is revealed using the electrochemical impedance analysis by applying the diluted electrode method. As the particle size of LMO increases, R_{cont} slightly decreases. The R_{ct} more strongly depends on the LMO particle size because of the change in specific surface area as a function of the particle size, although the charge transfer resistance per LMO surface area is constant. From the two resistances determined by the electrochemical impedance spectroscopy, the optimum particle morphology and electrode structure is discussed.

Keywords: lithium-ion battery; lithium manganese oxide; electrochemical impedance spectroscopy, diluted electrode method

1. Introduction

To achieve high-power lithium-ion batteries for automobile and stationary applications, the resistance of lithium insertion electrode has to be reduced because it is the main source of internal resistance of the battery. Since the lithium insertion electrodes used in lithium-ion batteries are porous electrodes, in which a lithium insertion material (as an active material), a carbon additive, and a polymer binder are mixed, there are two kinds of approaches for reducing the resistance of these electrodes; modifying the active material and designing the electrode structure. Most of the former approaches include the application of nano-sized materials [1], because it increases the surface-area-to-volume ratio of the active material. In the latter approach, the electrode becomes thinner and/or because resistance per active material weight decreases with decreasing electrode thickness [2-6].

Although these methods contribute to the resistance reduction of electrodes and lead to the development of high-power batteries, the electrode kinetics of lithium insertion electrodes are still unclear, because they do not separate the resistance of electrode into each component clearly, such as charge transfer resistance, contact resistance, ionic resistance, and electronic resistance [7-15]. Among these, the charge transfer and contact resistances are the main types of resistances in the lithium insertion electrodes. The charge transfer resistance is caused by the lithium insertion reaction that occurs on the active material surface, and the contact resistance occurs at the interface between the porous electrode and the current collector. Thus, the effects of physicochemical properties of active materials (such as particle size, surface area, and crystallinity) upon the resistances are particularly important to understand the electrode kinetics and improve the power-

capability of lithium insertion electrodes.

In our previous study [15], we succeeded in separating the two resistive components of electrodes by applying the diluted electrode method. In this method, the amount of active material can be systematically changed while retaining the factors related to electrode structure, such as the electrode weight, thickness and porosity [15,16]. Since the charge transfer resistance depends on the amount of active material and the contact resistance does not, resistance of an electrode can be divided into two resistive components by examining the diluted electrodes as a function of active material ratio. Therefore, the diluted electrode method allows to quantitatively clarify the contribution of charge transfer resistance and contact resistance to the resistance of lithium insertion electrode. This method also determines the relationship between the two resistances and the physicochemical properties of lithium insertion material.

In this study, we aimed to quantitatively clarify the relationship between the particle size of lithium manganese oxide ($Li[Li_{0.1}Mn_{1.9}]O_4$; LMO) and the resistive components of electrodes using the diluted electrode method. Dilute LMO electrodes with various active material ratios were prepared, and the electrochemical impedance was performed to examine the correlation between the particle size of LMO and the resistive components of the electrode. In addition, the method to design high-power lithium insertion electrodes was discussed according to the quantitative relationship between each resistive component and particle size.

2. Experiment method

2.1 Synthesis and characterization of lithium manganese oxide with different particle sizes

$Li[Li_{0.1}Mn_{1.9}]O_4$ (LMO) was synthesized using $LiOH \cdot H_2O$ (Kishida Chem. Co., Ltd.) and MnOOH (Tosoh). Raw materials were mixed with the ratio $LiOH \cdot H_2O$: MnOOH = 1.1 : 1.9. The mixed raw materials were calcined in air either at 1000 or 1100 °C for various hours. The synthesized samples were characterized by powder X-ray diffraction measurements using an X-ray diffractometer (XRD-6100, Shimadzu, Co. Ltd., Japan). The X-ray source was an iron tube (wavelength; λ = 1.93579 Å) and the tube voltage and current were 40 kV and 15 mA, respectively. The measurement range was 10 ° to 105 ° in 2θ at a scan rate of 0.5 ° min^{-1}. Particle shape of the samples was observed using SEM (VE-7800, Keyence Co., Ltd., Japan). Particle size distribution was determined by a particle size analyzer (LS13 320, Beckman Coulter Inc., USA).

2.2 Preparation of electrodes and electrochemical measurements

LMO and lithium titanium oxide $Li[Li_{1/3}Ti_{5/3}]O_4$ (LTO, Ishihara Sangyo Kaisha, LT855-17C) were used as the active materials. Alumina powder (Al_2O_3, Wako Pure Chemical Industries, Ltd.), acetylene black (AB), and polyvinylidene fluoride (PVdF) were used as a spectator material, a conductive additive, and a polymer binder, respectively. The diluted LMO electrodes consisted of LMO, Al_2O_3, AB, and PVdF in a mass ratio of x : 88 – x : 6 : 6. Al_2O_3 and AB were added to LMO, and the mixture was ground with a mortar and pestle for 10 min. PVdF dissolved in *N*-methylpyrrolidone (NMP) was added to the mixture to obtain a slurry. The slurry was spread onto an

aluminum foil with a blade and dried under vacuum at 80 °C for 1 h. The temperature was then raised to 150 °C and retained for 12 h. Finally, 2-cm^2 sections of the dried electrode were cut out with a hole punch.

The electrochemical behavior of the diluted LMO electrode was examined in lithium-ion cells with an LTO negative electrode, partially reduced in a lithium cell, prior to cell fabrication. Details of electrochemical cells and the instrumentation used for cell performance tests have been described previously [15,16]. Electrochemical impedance was measured using a 1260 frequency response analyzer (Solartron Analytical, West Sussex, U. K.) with a 1287 potentiostat. A sinusoidal voltage with a peak amplitude of 14.1 mV (RMS value = 10 mV) was superimposed on the open-circuit voltage (OCV) of the cell. The frequency was scanned stepwise, at 10 steps per decade from 100 kHz to 10 mHz.

2.3 Calculation of electrochemical impedance of a single LMO electrode

Impedance of a single LMO electrode was obtained the same way described previously [15], i.e., subtracting the impedance of a single LTO electrode from the impedance of an LTO/LMO cell.

$$Z_{LMO} = Z_{Cell} - Z_{LTO} = Z'_{Cell} - Z'_{LTO} + i(Z''_{Cell} - Z''_{LTO}) \quad (1)$$

The impedance of a single LTO electrode can be measured in an LTO/LTO symmetric cell composed of two LTO electrodes with identical weight and thickness [17-20]. The LTO/LTO symmetric cell was prepared using fully-oxidized and fully-reduced LTO

electrodes prepared in lithium cells, which were disassembled and combined in a flesh cell. The electrochemical behaviors of both LTO electrodes, such as reversible capacity, polarization, and impedance are consequently identical. The electrochemical impedance of the LTO/LTO symmetric cells were measured at 50% state of charge of the cell, where the chemical composition of LTO electrodes ($Li_{3/2}[Li_{1/3}Ti_{5/3}]O_4$) was identical. Hence, the impedance of a single LTO electrode was calculated to be half of the symmetric cell as shown in equation (2).

$$Z_{LTO} = Z_{LTO/LTO} / 2 \quad (2)$$

3. Results and Discussion

3.1 Lithium manganese oxide with different particle sizes

Fig. 1 shows the X-ray diffraction (XRD) patterns of LMO calcined under various conditions. The diffraction lines of all the XRD patterns were assigned to cubic lattices and virtually located at the same diffraction angles. Their lattice constants calculated by the least squares method were approximately 8.22 Å, which are similar to those of LMO reported previously (8.215 Å) [21,22]. The SEM images (Fig. 2) show that all the samples have smooth facets and micrometer-size particles. The LMO calcined at 1100 °C, which was the largest crystal, had particles of approximately 10 μm or larger. In all the XRD patterns, diffraction lines are too narrow to evaluate the crystallite size by Scherrer equation; full-width at half-maximum (FWHM) is less than 0.2 °. The crystallite size was estimated by the particle size distribution measurement (Fig. 3). The mean particle size

D_{50} was 5.0 μm at 1000 °C for 2 h, 6.8 μm at 1000 °C for 15 h, 8.3 μm at 1000 °C for 50 h, and 8.9 μm at 1100 °C for 4 h. Therefore, the LMO particles having different particle sizes could be synthesized by increasing either the calcination time or the calcination temperature.

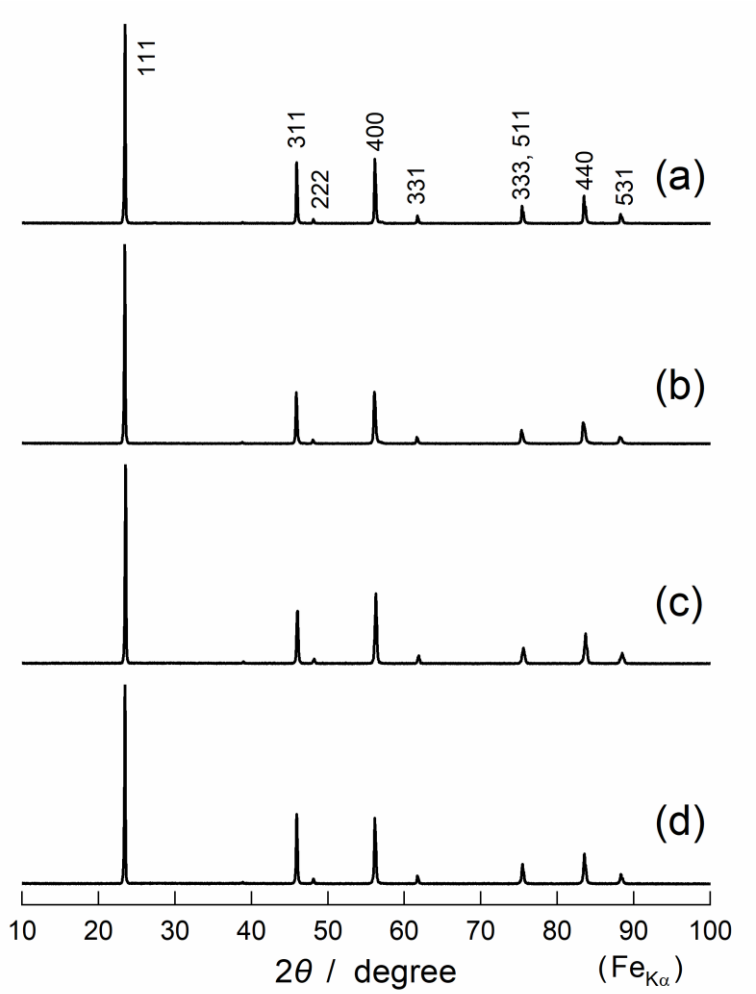

Fig. 1. XRD patterns of $Li[Li_{0.1}Mn_{1.9}]O_4$ calcined at 1000 °C for (a) 2 h, (b) 15 h, (c) 50 h, and (d) at 1100 °C for 4 h in air.

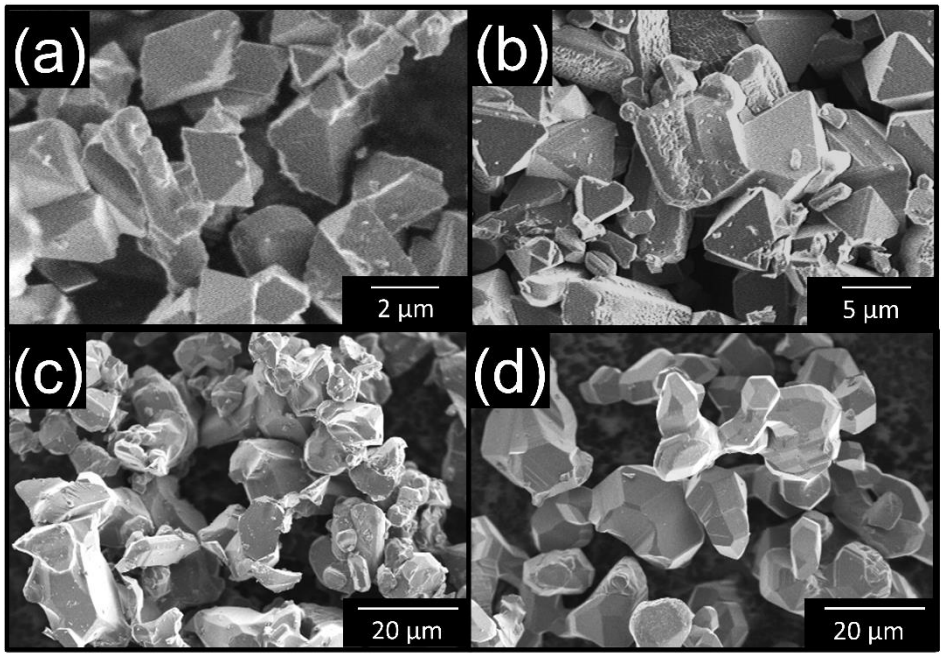

Fig. 2. SEM images of $Li[Li_{0.1}Mn_{1.9}]O_4$ particles calcined at 1000 °C for (a) 2 h, (b) 15 h, (c) 50 h, and (d) at 1100 °C for 4 h in air.

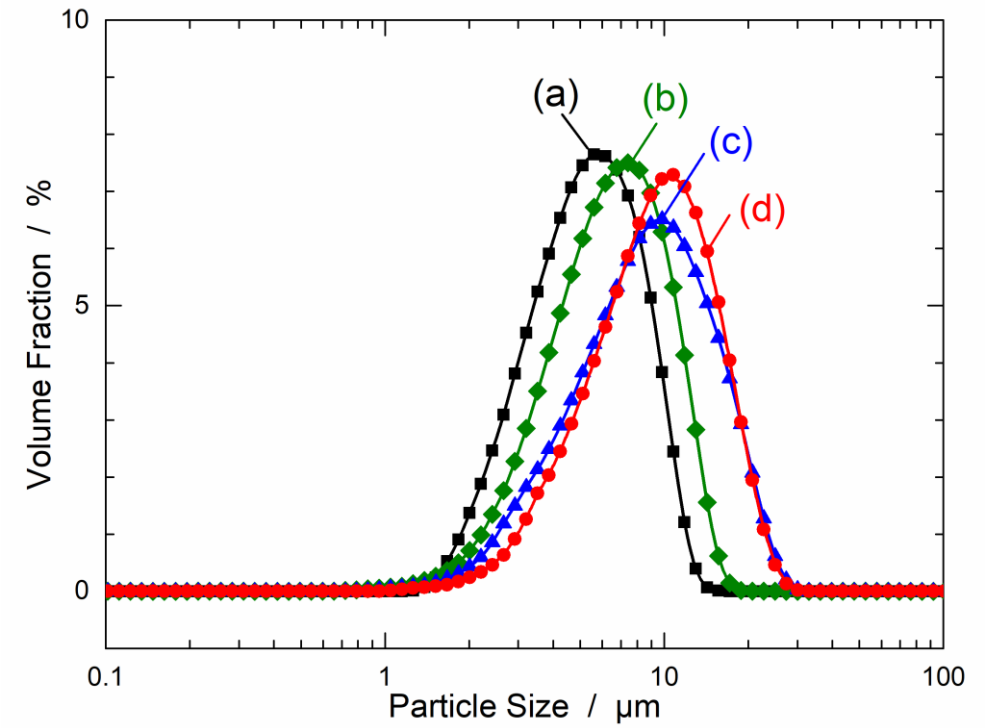

Fig. 3. Particle size distribution of LMO calcined at 1000 °C for (a) 2 h, (b) 15 h, (c) 50 h, and (d) at 1100 °C for 4 h in air.

Fig. 4 shows the results of charge-discharge curves of the LMOs examined in a half cell configuration with a lithium-metal counter electrode. All the samples reacted at 4 V with a reversible capacity of 97-105 mAh g^{-1}. The electrochemical reaction of LMO ($Li[Li_xMn_{2-x}]O_4$) can be expressed by equation (3), assuming that the solid-state redox reaction of Mn^{3+}/Mn^{4+} proceeds.

$$Li[Li_xMn_{2-x}]O_4 \rightleftarrows Li_{3x}[Li_xMn_{2-x}]O_4 + (1-3x)Li^+ + (1-3x)e^- \quad (3)$$

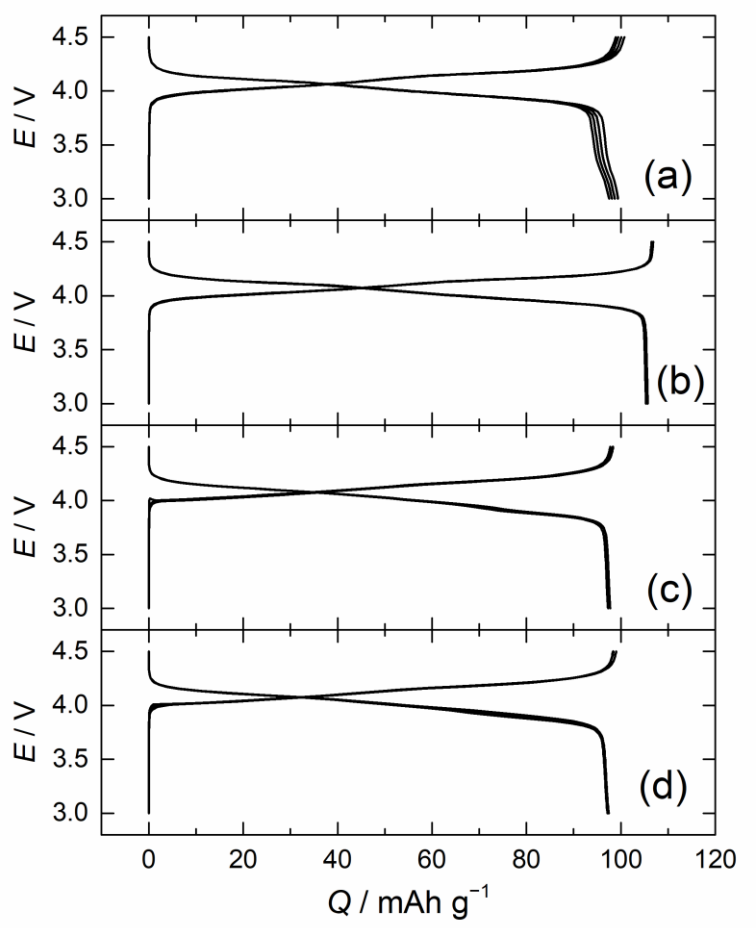

Fig. 4. Charge-discharge curves of Li / LMO cells operated at 0.5 mA cm^{-2} in the voltage range 3.0 to 4.5 V. LMO calcined at 1000 °C for (a) 2 h, (b) 15 h, (c) 50 h, and (d) at 1100 °C for 4 h. The LMO electrodes consisted of LMO : AB : PVdF = 88 : 6 : 6.

According to the equation (3), the theoretical capacity of $Li[Li_xMn_{2-x}]O_4$ strongly depends on x. In the case of LMO with $x = 0.1$, the equation (3) can be rewritten as follows.

$$Li[Li_{0.1}Mn_{1.9}]O_4 \rightleftarrows Li_{0.3}[Li_{0.1}Mn_{1.9}]O_4 + 0.7Li^+ + 0.7e^- \quad (4)$$

The theoretical capacity of LMO (x = 0.1) is $Q = 107$ mAh g^{-1}. If $x = 0.12$, the theoretical capacity is calculated to be 95 mAh g^{-1}. The value of x was calculated to be approximately 0.10–0.12, from the measured reversible capacity, based on the equation (4). Consequently, the chemical composition of LMOs was approximately $Li[Li_{0.1}Mn_{1.9}]O_4$ with negligible deviation of x.

3.2 Electrochemical impedance spectra of diluted LMO electrodes

Diluted electrodes prepared by mixing the LMO and aluminum oxide powder at various ratios were employed for charge-discharge tests using a lithium-ion cell with an LTO-negative electrode. Fig. 5 shows the results of LMO calcined at 1000 °C for 15 h. No significant differences were observed in the operating voltage, the voltage shape, and the reversible capacity of all the electrodes. This indicates that the aluminum oxide (as a spectator material) in diluted electrode does not affect the electrochemical behavior of LMO.

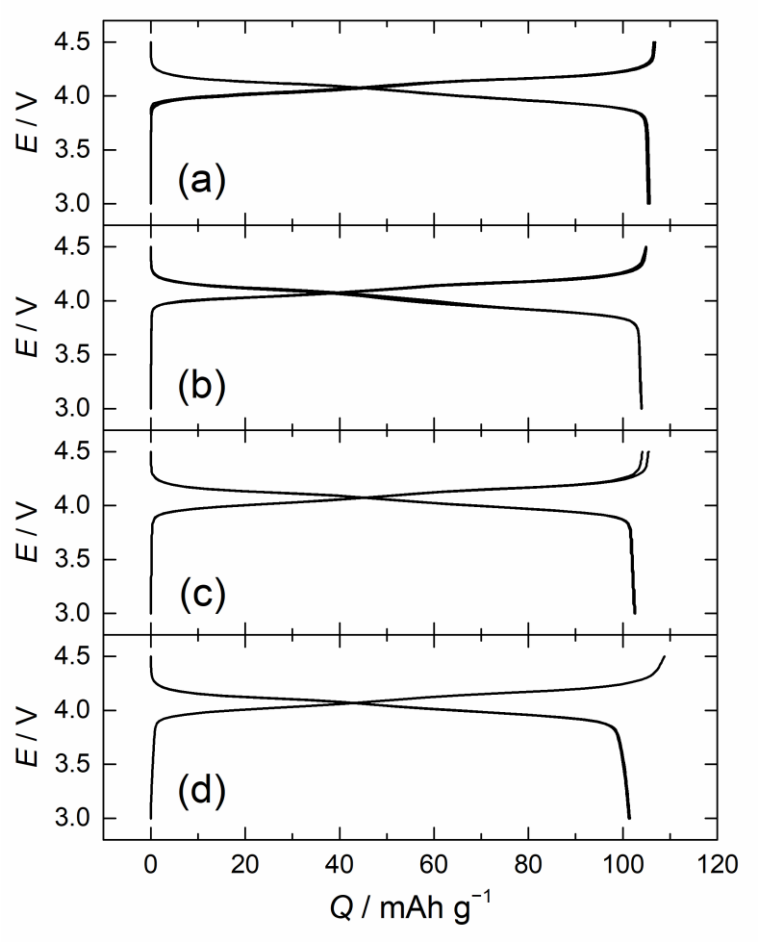

Fig. 5. Charge and discharge curves of Li / LMO cells operated at 0.5 mA cm^{-2} in the voltage range 3.0 to 5.0 V. The LMO calcined at 1000 °C for 15 h in air. LMO electrodes consisted of LMO : Al_2O_3 : AB : PVdF = x : 88−x : 6 : 6 (wt%) [(a) x = 88, (b) x = 44, (c) x = 22, or (d) x = 6].

Fig. 6 shows the Nyquist plots of impedance measurements of the diluted LMO electrodes obtained by subtracting Z_{LTO} from Z_{Cell}. The impedance spectra were measured at 30% state of charge of the LMO. In LMO, impedance is almost constant in the range of 10-90% SOC [23, 24]. In all the Nyquist plots, two semicircles appeared in the high and low frequency ranges. In the previous study on diluted electrodes [11], the semicircles

in high frequency corresponded to the contact resistance R_{cont}, and that in low frequency to the charge transfer resistance R_{ct}. The value of R_{cont} observed in the high frequency region was approximately 2–4 Ω. This means, the R_{cont} showed a slight, but systematic change depending on the LMO particle size; the R_{cont} decreased as the particle size increased. In contrast, the R_{ct} observed in the low frequency region became larger as the LMO content became smaller. The R_{ct} strongly depends on the particle size, because smaller particle size results in larger reaction surface area.

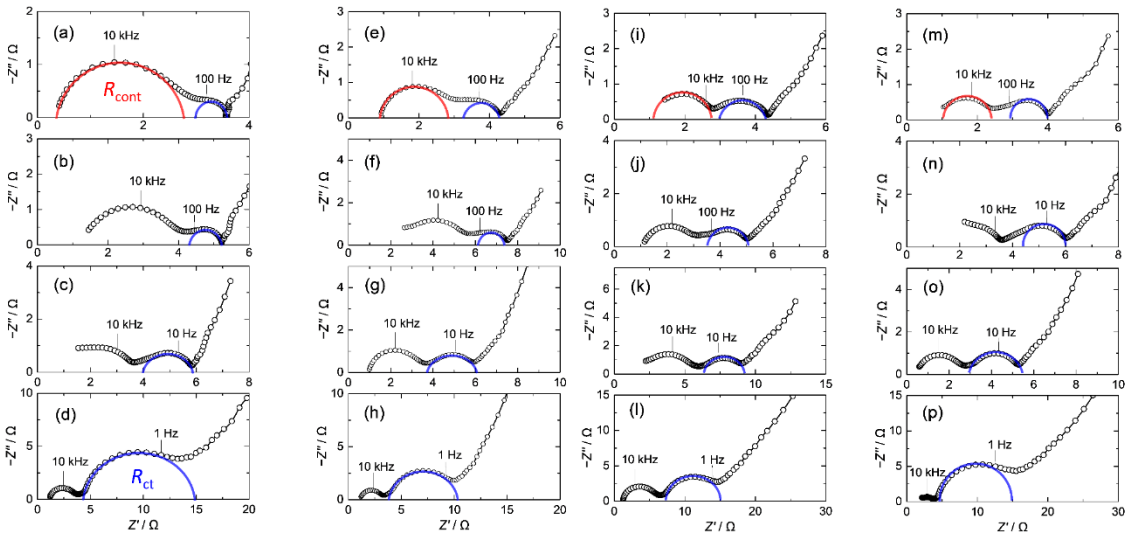

Fig. 6. The Nyquist plots of LTO / diluted LMO cells. LMO calcined at 1000 °C for (a-d) 2 h, (e-h) 15 h, (i-l) 50 h, and (m-p) at 1100 °C for 4 h in air. The diluted LMO electrodes consisted of LMO : Al_2O_3 : AB : PVdF = x : 88−x : 6 : 6 (wt%) [(a, e, i, m) x = 88, (b, f, j, n) x = 44, (c, g, k, o) x = 22, and (d, h, l, p) x = 6]. The amplitude of sinusoidal voltage is 10 mV. The impedance spectra of the cells were measured at 30% of the state of charge.

The R_{cont} of LMO electrodes with 88 wt% LMO content was plotted against the particle size (Fig. 7). The contact resistance was clearly dependent on the particle size; the larger the particle size, the smaller the R_{cont}. The resistance of the larger sample approximately reduced to half of the smaller sample (2.7 Ω for the LMO calcined at 1100 °C and 4.8 Ω for the LMO calcined at 1000 °C for 2 h). This result is consistent with a previous report, in that high crystalline particles have excellent output characteristics in LiNiMO having the same crystal structure and particle shape [25].

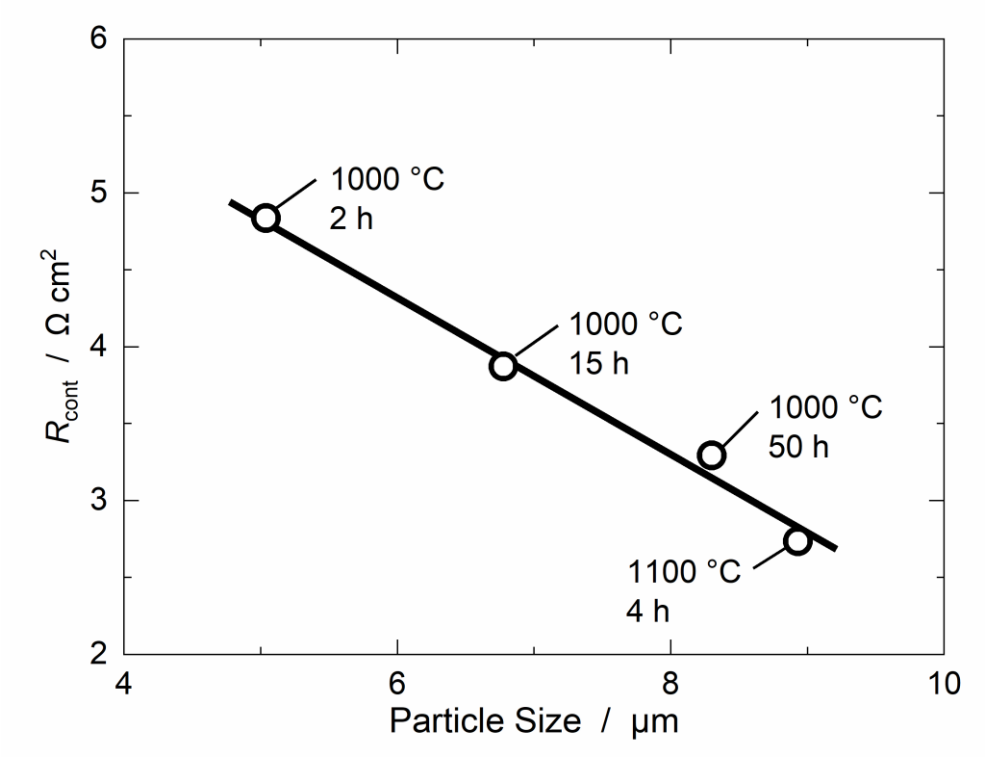

Fig. 7. Contact resistance R_{cont} of LMO electrodes as a function of LMO particle size. R_{cont} was estimated from the radius of semicircles in high-frequency region in the Nyquist plots (Fig. 6).

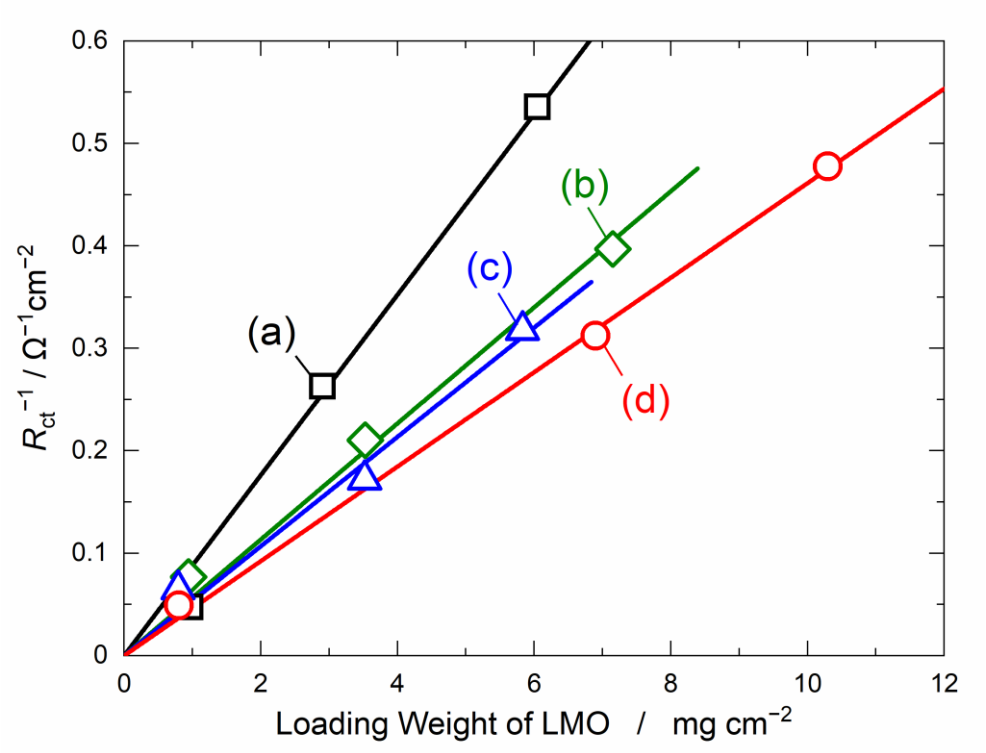

Fig. 8. The reciprocal of charge transfer resistance R_{ct}^{-1} of the diluted LMO electrodes as a function of the loading weight of LMO in the electrodes. LMO calcined at 1000 °C for (a) 2 h, (b) 15 h, (c) 50 h, and (d) at 1100 °C for 4 h in air.

Fig. 8 shows the reciprocal of R_{ct} determined from the radius of semicircles in low frequency region, plotted against the LMO content. There was a proportional relationship between the inverse of R_{ct} and the LMO content. However, when the LMO content is high, the R_{ct} is larger than expected from a linear relationship and does not follow the line. Therefore, these data are excluded to fit the equation, representing the proportional relationship. This shift is considered to be caused by the ionic resistance in the pores of

diluted electrodes, which is another resistive component other than the R_{ct} [9,10]. When the amount of active material is small, the contribution of unexpected resistance existing in the low-frequency semicircles is relatively small, because the R_{ct} depending on the LMO content is large. However, when the LMO content is large, resulting in small R_{ct}, the resistance due to other factors becomes relatively large compared to the R_{ct}. Consequently, the R_{ct} values of the diluted electrodes with 88 wt% LMO content are not on the straight line. The influence of resistive components other than the R_{ct} will be discussed later.

From Fig. 8, the value of charge transfer resistance per unit weight of the material, $R_{ct,W}$, was calculated from the slopes of straight lines. The slope increases with increasing particle size, indicating that LMO with small particle size has low resistance, $R_{ct,\,W}$ [Ω g]. Fig. 9a shows $R_{ct,\,W}$ plotted against the particle size. The $R_{ct,\,W}$ of larger LMO is twice the $R_{ct,\,W}$ of smaller LMO; the highest being 70 Ω^{-1} g^{-1} and the lowest 32 Ω^{-1} g^{-1}. The power capability per unit mass is obviously dependent on the particle size, because the smaller the particle size, the larger the surface area per unit weight.

To compare the charge transfer resistance per surface area, $R_{ct,\,A}$ of the LMO particles, the specific surface area of the material was estimated from the particle size measured by the particle size distribution. The XRD density of the unit cell is expressed by the following equation.

$$\text{XRD density} = \frac{\text{F.W.}}{a^3/8 \times N_A} \qquad (5)$$

where, F.W. is the formula weight, a is the lattice constant of LMO, and N_A is the

Avogadro's number. When the particle morphology is approximated as spherical, the particle volume is $4\pi r^3/3$ (r is the particle radius) . Therefore, surface area per unit mass is obtained by the following equation.

$$\frac{\text{surface area}}{\text{mass}}\,[\text{m}^2\ \text{g}^{-1}] = \frac{\text{surface area}\ [\text{m}^2\ \text{mol}^{-1}]}{\text{volume}\ [\text{cm}^3\ \text{mol}^{-1}] \times \text{XRD density}\ [\text{g}\ \text{cm}^{-3}]} \qquad (6)$$

Using the specific surface area and the $R_{\text{ct, W}}$, the charge transfer resistance based on the surface area of LMO, $R_{\text{ct, A}}$ can be calculated.

$$R_{\text{ct, A}}\ [\Omega\ \text{m}^2] = R_{\text{ct,W}}\ [\Omega\ \text{g}] \times \frac{\text{surface area}}{\text{mass}}\,[\text{m}^2\ \text{g}^{-1}] \qquad (7)$$

The $R_{\text{ct, A}}$ of LMO particles was calculated with the equation (7) and plotted against the particle size (Fig. 9b). The $R_{\text{ct, A}}$ was almost a constant value (*ca.* 1.7 mΩ m^2) regardless of the particle size. Therefore, the charge transfer resistance per unit surface area was virtually same for all the LMO particles.

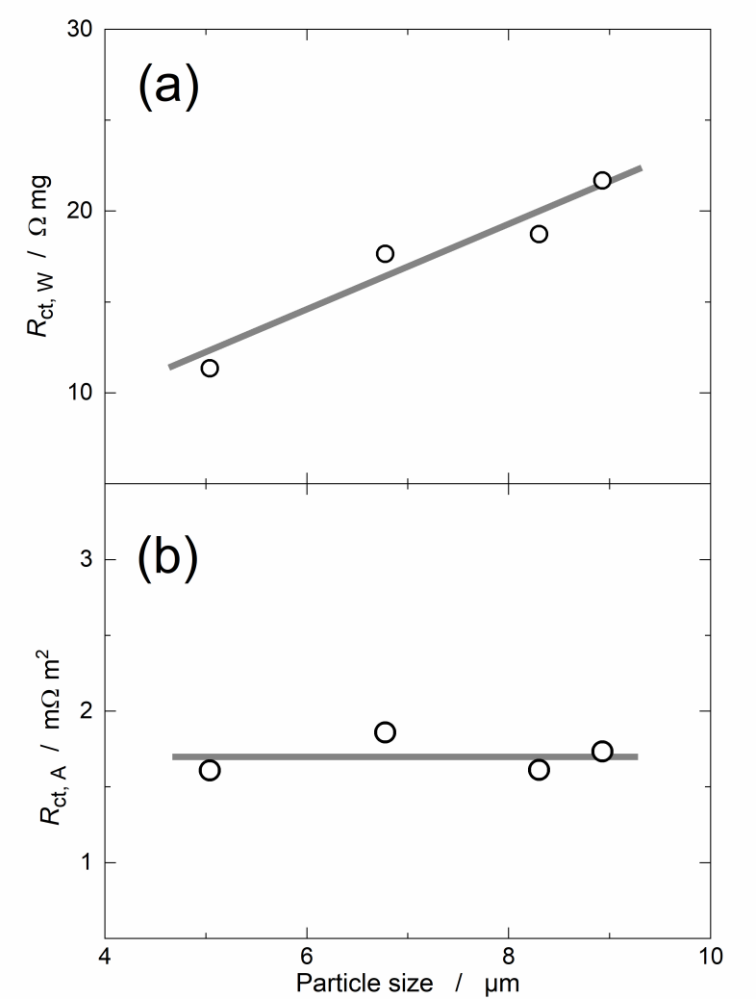

Fig. 9. Charge transfer resistance per (a) LMO weight ($R_{ct, W}$) or (b) LMO surface area ($R_{ct, A}$) as a function of the LMO particle size.

3.3 Dependence of particle size on the total resistance of LMO electrodes, as a function of loading weight

In the previous section, the dependences of particle size upon R_{ct} and R_{cont} were determined by using the diluted electrode method. As the particle size increases, the R_{cont} decreases, while the R_{ct} increases. Assuming that the total resistance of electrode is the

sum of these two resistances, the resistance per unit geometric area of the electrode, R_A can be calculated from the two resistances and the loading weight. If the electrode density is constant, the loading weight is proportional to the electrode thickness. Thus, the total resistance of electrode is a function of the electrode thickness. The R_{cont} is constant, independent of the loading weight and electrode thickness. However, the R_{ct} exhibits loading weight dependence. Therefore, the total resistance can be calculated by the following formula.

$$R_A = R_{cont} + R_{ct} = R_{cont} + R_{ct,\,W} \times (\text{loading weight}) \qquad (8)$$

The R_A of LMO electrode with various particle sizes was calculated using the equation (8), and the obtained values of R_A were plotted against the loading weight (Fig. 10). When the loading weight is extremely low (thinner electrode), the R_{ct} has a large value because the amount of LMO is extremely small. Therefore, the R_A is large and the difference is slight, even if the LMO with small particle size is used. In contrast, when the loading weight is large (thicker electrode), the amount of LMO increases, so the R_{ct} decreases. The R_{cont} is independent of the amount of LMO. Therefore, for thick electrodes, the contribution of R_{ct} to R_A is extremely small, and most of it is determined by R_{cont}. Hence, the LMO with large particle size is appropriate to reduce the resistance of thick electrode.

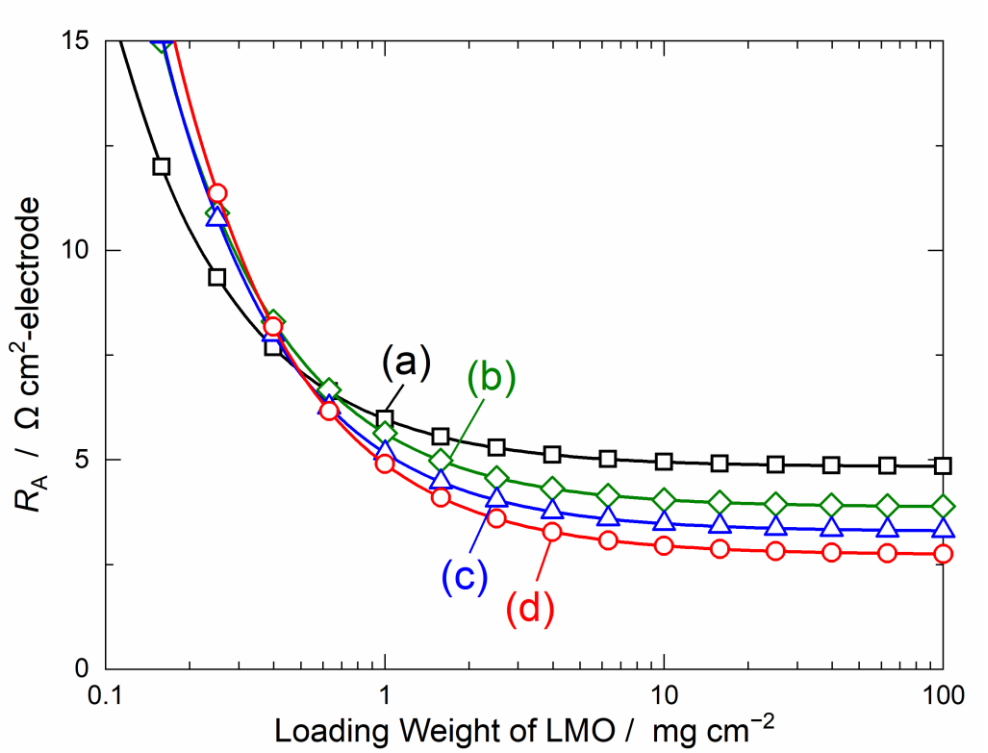

Fig. 10. Plots of the total resistance of LMO electrodes, R_A against the loading weight of LMO. R_A is calculated from the sum of R_{cont} and R_{ct}.

When the resistance per unit mass of the active material is considered, the overall resistance is smaller because the electrode area of the thin electrode is larger. However, the thinner the electrode is, the larger the proportion of battery components, such as current collector and separator. Thus, it does not lead to an improvement directly in the power density of the battery. However, the thicker the electrodes, the more negligible their weight will be, resulting in improved power density [26-30]. Consequently, thick electrodes with large sized LMO particles are believed to be appropriate to improve the power density of the battery. Here, only the charge transfer resistance and the contact resistance are considered. The resistance caused by the ionic conduction in electrode is

not considered. It has been reported that the ionic resistance largely contributes in thicker electrodes [9,10]. In fact, the experimental results of this paper also show that the resistance of electrode becomes larger than the expected value of R_{ct} when the electrode has a large amount of LMO. Therefore, in order to design a high-power electrode, it is necessary to consider the ionic resistance in electrode. The quantitative analysis of the contribution of ionic resistance in a thick electrode, and the calculation of the internal resistance of electrode considering ionic resistance are currently being performed in our laboratory. If this attempt is successful, it is expected to obtain more precise and accurate design guidelines for high power electrodes.

4. Conclusion

By applying the diluted electrode method to $Li[Li_{0.1}Mn_{1.9}]O_4$ (LMO), we revealed the impact of the particle size of LMO on the charge transfer resistance R_{ct} (appeared in the low-frequency region) and the contact resistance R_{cont} (appeared in the high-frequency region) using the electrochemical impedance spectra. The R_{cont} derived from the interface between the porous electrode and the current collector slightly correlates with the particle size; large particles show smaller R_{cont}. However, the R_{ct} strongly depends on the particle size, the smaller the particle size, the lower the R_{ct}. This is consistent with the expectation based on the volume-to-area ratio. The charge-transfer resistance per LMO surface area, $R_{ct,A}$ estimated from the R_{ct} and the XRD density of LMO is constant, regardless of the difference in crystallinity of the materials. This suggests that the large secondary particles which consists of small aggregated primary particles, form the optimum active material

required for a high-power electrode. Furthermore, from the dependence of R_{ct} and R_{cont} on the particle size, an electrode structure suitable for high output was discussed; a thick electrode composed of large particles, possibly improves the power capability of LMO electrodes.

Acknowledgement

This work was supported by JSPS KAKENHI Grant Number 20K05687.

References

[1] P. G. Bruce, B. Scrosati, and J.-M. Tarascon, Angew. Chem. Int. Ed. 47 (2008) 2930.

[2] W. Lu, A. Jansen, D. Dees, P. Nelson, N. R. Veselka, and G. Henriksen, J. Power Sources 196 (2011) 1537.

[3] H. Zheng, J. Li, X. Song, G. Liu, and V. S. Battaglia, Electrochim. Acta 71 (2012) 258.

[4] G. Inoue and M. Kawase, J. Power Sources 342 (2017) 476.

[5] L. Liu, P. Guan, and C. Liu, J. Electrochem. Soc. 164 (2017) A3163.

[6] C. Heubner, A. Nickol, J. Seeba, S. Reuber, N. Junker, M. Wolter, M. Schneider, and A. Michaelis, J. Power Sources 419 (2019) 119.

[7] J. M. Atebamba, J. Moskon, S. Pejovnik, and M. Gaberscek, J. Electrochem. Soc. 157 (2010) A1218.

[8] N. Ogihara, S. Kawauchi, C. Okuda, Y. Itou, Y. Takeuchi, and Y. Ukyo, J. Electrochem. Soc. 159 (2012) A1034.

[9] N. Ogihara, Y. Itou, T. Sasaki, and Y. Takeuchi, J. Phys. Chem. C 119 (2015) 4612.

[10] Y. Orikasa, Y, Gogyo, H. Yamashige, M. Katayama, K. Chen, T. Mori, K. Yamamoto, T. Masese, Y. Inada, T. Ohya, Z. Shiroma, S. Kato, H. Kinoshita, H. Arai, Z. Ogumi, and Y. Uchimoto, Scientific reports 6 (2016) 26382.

[11] Z. Siroma, T. Sato, T. Takeuchi, R. Nagai, A. Ota, and T. Ioroi, J. Power Sources 316 (2016) 215.

[12] T. Fukutsuka, K. Koyamada, S. Maruyama, K. Miyazaki, and T. Abe, Electrochim. Acta 199 (2016) 380.

[13] M. Takeno, T. Fukutsuka, K. Miyazaki, and T. Abe, J. Electrochem. Soc. 164 (2017) A3862.

[14] A. S. Keefe, S. Buteau, I. G. Hill, and J. R. Dahn, J. Electrochem. Soc. 166 (2019) A3272.

[15] K. Ariyoshi, S. Mizutani, and Y. Yamada, J. Power Sources 435 (2019) 226810.

[16] K. Ariyoshi, S. Mizutani, T. Makino, and Y. Yamada, J. Electrochem. Soc. 165 (2018) A3965.

[17] C. H. Chen, J. Liu, and K. Amine, J. Power Sources 96 (2001) 321.

[18] T. Ohzuku, R. Yamato, T. Kawai, and K. Ariyoshi, J. Solid State Electrochem. 12 (2008) 979.

[19] K. Nakura, K. Ariyoshi, F. Ogaki, K. Takaoka, and T. Ohzuku, J. Electrochem. Soc. 161 (2014) A841.

[20] I. J. Gordon, S. Genies, G. S. Larbi, A. Boulineau, L. Daniel, and M. Alias, J. Power Sources 307 (2016) 788.

[21] T. Ohzuku, S. Kitano, M. Iwanaga, H. Matsuno, and A. Ueda, J. Power Sources 68 (1997) 646.

[22] G. G. Amatucci, N. Pereira, T. Zheng, and J. M. Tarascon, J. Electrochem. Soc. 148 (2001) A171.

[23] K. Dokko, M. Mohamedi, M. Umeda, and I. Uchida, J. Electrochem. Soc. 150 (2003) A425.

[24] I. Yamada, K. Miyazaki, T. Fukutsuka, Y. Iriyama, T. Abe, and Z. Ogumi, J. Power Sources 294 (2015) 460.

[25] K. Ariyoshi, Y. Maeda, T. Kawai, and T. Ohzuku, J. Electrochem. Soc. 158 (2011) A281.

[26] Z. Du, D. L. Wood, C. Daniel, S. Kalnaus, and J. Li, J. Appl. Electrochem. 47 (2017) 405.

[27] H. Gao, Q. Wu, Y. Hu, J. P. Zheng, K. Amine, and Z. Chen, J. Phys. Chem. Lett. 9 (2018) 5100.

[28] X. Wu, S. Xia, Y. Huang, X. Hu, B. Yuan, S. Chen, Y. Yu, and W. Liu, Adv. Funct. Mater. 29 (2019) 1903961.

[29] Z. Nie, P. McCormack, H. Z. Bilheux, J. C. Bilheux, J. P. Robinson, J. Nanda, and G. M. Koenig Jr, J. Power Sources 419 (2019) 127.

[30] J. Hu, B. Wu, X. Cao, Y. Bi, S. Chae, C. Niu, B. Xiao, J. Tao, J. Zhang, and J. Xiao, J. Power Sources, 454 (2020) 227966.